Phase Behavior of Mixtures of Oppositely Charged Nanoparticles: Heterogeneous Poisson−Boltzmann Cell Model Applied to Lysozyme and Succinylated Lysozyme

P. Maarten Biesheuvel, Saskia Lindhoud, Renko de Vries, and Martien A. Cohen Stuart

Laboratory of Physical Chemistry and Colloid Science, Wageningen University, Dreijenplein 6, 6703 HB Wageningen, The Netherlands

Received August 26, 2005. In Final Form: November 14, 2005

We study the phase behavior of mixtures of oppositely charged nanoparticles, both theoretically and experimentally. As an experimental model system we consider mixtures of lysozyme and lysozyme that has been chemically modified in such a way that its charge is nearly equal in magnitude but opposite in sign to that of unmodified lysozyme. We observe reversible macroscopic phase separation that is sensitive not only to protein concentration and ionic strength, but also to temperature. We introduce a heterogeneous Poisson−Boltzmann cell model that generally applies to mixtures of oppositely charged nanoparticles. To account for the phase behavior of our experimental model system, in addition to steric and electrostatic interactions, we need to include a temperature-dependent short-ranged interaction between the lysozyme molecules, the exact origin of which is unknown. The strength and temperature dependence of the short-ranged attraction is found to be of the same order of magnitude as that between unmodified lysozyme molecules. The presence of a rather strong short-ranged attraction in our model system precludes the formation of colloidal liquid phases (or complex coacervates) such as those typically found in mixtures of globular protein molecules and oppositely charged polyelectrolytes.

Introduction

Solutions of colloidal spheres, with sizes from hundreds of nanometers down to a few nanometers have been used extensively as models for simple liquids. Conversely, theories of simple liquids have been used to interpret experiments on suspensions of colloidal spheres, including solutions of globular proteins.

Colloidal analogues have not yet been widely studied for A+B mixtures in which A−A and B−B interactions are repulsive, but A−B interactions are attractive, such as in electrolyte solutions. Above a critical coupling strength, electrolyte solutions exhibit phase transitions to dense phases, which have been the subject of renewed theoretical interest.[1] Mixtures of oppositely charged nanoparticles are a colloidal analogue of electrolyte solutions[2] that could provide novel ways to test theoretical predictions and provide a stimulus for further theoretical work, as demonstrated beautifully by recent results on crystal phases formed by oppositely charged colloids of dissimilar size.[3]

Mixtures of oppositely charged nanoparticles are also a convenient model system for electrostatic complexation in mixtures of oppositely charged macromolecules in general. Experimental studies have been performed for a wide variety of combinations of oppositely charged macromolecules. The multitude of parameters that come into play for the complicated mixtures that have been studied so far are a serious handicap in modeling efforts. These would be helped by experiments on systems with a smaller parameter space, such as a system of oppositely charged nanoparticles of a single radius and a charge that is equal in magnitude but opposite in sign.

With this in mind, we here present an exploratory experimental study of the phase behavior of mixtures of oppositely charged nanoparticles. More specifically, we use the protein lysozyme and its chemically modified analogue, succinylated lysozyme. These two globular molecules are rather spherical and virtually identical in size and shape, but differ in their net charge. By changing the pH, one can find conditions where the two molecules have a charge that is roughly equal in magnitude but opposite in sign. We also introduce a simple statistical thermodynamical model that generally applies to mixtures of oppositely charged nanoparticles. Electrostatic free energies are calculated using a heterogeneous Poisson−Boltzmann (PB) cell model, an extension of a previous model for the formation of complex coacervate phases in mixtures of oppositely charged flexible polyelectrolytes.[4]

Previous studies of mixtures of oppositely charged protein molecules[5−10] have mainly been concerned with cross-interactions under conditions where macroscopic phase separation does not yet take place. However, macroscopic phase separation for aqueous mixtures of two types of γ-crystallin, a lens protein, has been studied by Liu et al.[11,12] Compared to systems used in previous studies on oppositely charged globular protein molecules, our system has the simplicity that one requires of a model system: the two proteins species are identical, except for the chemical modification of the lysine and tyrosine residues at the surface of the succinylated protein. We can tune the pH to obtain a system in which the charges are almost equal in magnitude, but opposite in sign.

(1) Fisher, M. E.; Levin, Y. *Phys. Rev. Lett.* **1993**, *71*, 3826.
(2) Caballero, J. B.; Puertas, A. M.; Fernández-Barbero, A.; de las Nievas, F. J. *J. Chem. Phys.* **2004**, *121*, 2428
(3) Leunissen, M. E.; Christova, C. G.; Hynninen, A. P.; Royall, C. P.; Campbell, A. I.; Imhof, A.; Dijkstra, M.; van Roij, R.; van Blaaderen, A. *Nature* **2005**, *437*, 235.
(4) Biesheuvel, P. M.; Cohen Stuart, M. A. *Langmuir* **2004**, *20*, 4764.
(5) Steiner, R. F. *Arch. Biochem. Biophys.* **1953**, *46*, 291; **1953**, *47*, 56.
(6) McCarty, B. W.; Adams, E. T., Jr. *Biophys. Chem.* **1987**, *28*, 149.
(7) Moon, Y. U.; Curtis, R. A.; Anderson, C. O.; Blanch, H. W.; Prausnitz, J. M. *J. Solution Chem.* **2000**, *29*, 699.
(8) Nichol, L. W.; Winzor, D. J. *J. Phys. Chem.* **1964**, *68*, 2455.
(9) Howlett, G. J.; Nichol, L. W. *J. Biol. Chem.* **1973**, *248*, 619.
(10) Tessier, P. M.; Sandler, S. I.; Lenhoff, A. M. *Protein Sci.* **2004**, *13*, 1379.
(11) Liu, C.; Asherie, N.; Lomakin, A.; Pande, J.; Ogun, O.; Benedek, G. B. *Proc. Natl. Acad. Sci.* **1996**, *93*, 377.
(12) Liu, C.; Lomakin, A.; Thurston, G. M.; Hayden, D.; Pande, A.; Pande, J.; Ogun, O.; Asherie, N.; Benedek, G. B. *J. Phys. Chem.* **1995**, *99*, 454.

10.1021/la052334d CCC: $33.50
Published on Web 01/05/2006

Compared to much larger colloidal spheres, the present system has the advantage of much lower absolute values of the charge, such that we can get one-phase systems at reasonable ionic strengths. Additionally, the protein size is in the range of quite accessible Debye lengths in aqueous systems, such that both long-range and short-range interactions can be investigated. Our emphasis here is on a systematic study of the phase behavior to set the stage for studies probing the nature of the phases in more detail.

Materials and Methods

For details of the protein molecules used, namely hen egg-white lysozyme and its chemical modification, succinylated lysozyme, see ref 13. In analyzing the data, we assume a molar mass of 14.3 kDa for lysozyme and 15.2 kDa for succinylated lysozyme. Lysozyme has an isoelectric point of pI = 10.7, whereas the pI for succinylated lysozyme is 4.7.[13,14] The protein charge Z, as a function of pH, is known from titration data,[13] which corresponds well with a simple titration model.[14] At pH 7.5, lysozyme has about +7 charges, and succinylated lysozyme has about −7.

Proteins were dissolved in demineralized water, after which the pH was adjusted to 7.5. Before use, solutions were filtered through a 0.1 μm pore size filter, and the protein concentration was determined spectrophotometrically (281.5 nm; extinction coefficient $\epsilon = 2.635$ (liter·cm)/g). The ionic strength was adjusted using a concentrated stock solution of NaCl.

Three different experimental methods were used to determine the phase behavior.

Method I. Turbidity at 400 nm is measured in a stirred cell, during a titration of a 1 g/L lysozyme solution with a 1 g/L solution of succinylated lysozyme, or vice-versa. The phase boundary is identified with the point at which transmission has decreased from 100% to 95%.

Method II. Mixed protein solutions were equilibrated for 1 h, centrifuged for 1 h at 12,000 rpm, and left to equilibrate for another hour, after which the protein concentration of the supernatant was determined spectrophotometrically as described above.

Method III. Solutions are prepared in capped glass tubes and placed in a stirred water bath. The temperature of the bath is increased in one-degree increments. After stabilization of the temperature and an additional hold time of 2 min, we visually determine whether the sample has become transparent or not. In this way we determine the clarification temperature, $T_{clarify}$, above which the sample becomes transparent.

Experimental Results

In a first set of experiments, we vary the mixing ratio between the positive lysozyme and the negative succinylated lysozyme at a fixed total concentration of protein of $c = 1$ g/L. At each ionic strength, we determine the two critical values (at low and high lysozyme concentration) by Method I (see Figure 1). Not unexpectedly for our nearly perfectly symmetric system, the extent of phase separation is largest at a mass mixing ratio of $f^+ = c^+/c \approx 0.5$ (where c^+ is the mass concentration of lysozyme). What is more surprising is that phase separation persists down to extremely asymmetric mixing ratios. This is different, for example, in mixtures of oppositely charged polyelectrolytes, where phase separation occurs in a much narrower range of mixing ratios, around $f^+ \approx 0.5$.[15] Most likely, this is related to the nearly perfect symmetry of our system, in terms of both the magnitude of the charges, and the geometry of the charged objects. This symmetry probably excludes the formation of small soluble aggregates with a stabilizing net charge, as occurs when charge densities and geometries of the positive and negative macromolecules are sufficiently different.

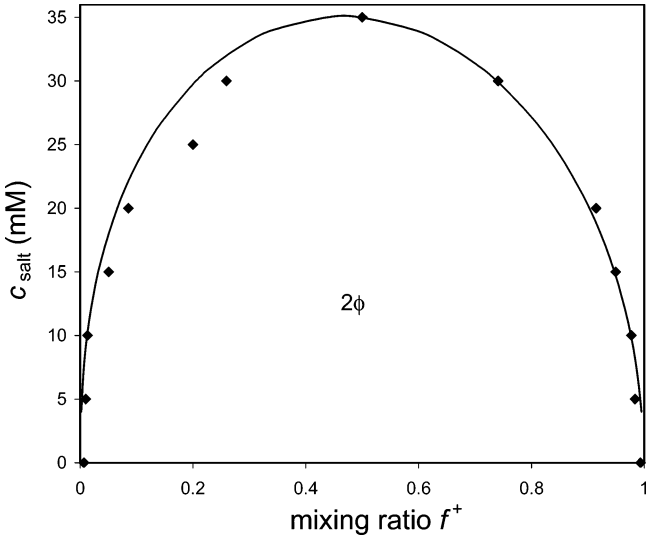

Figure 1. Critical ionic strength as a function of protein mixing ratio, f^+, for 1 g/L total protein concentration. 2ϕ denotes the two-phase region. Experimental data obtained via Method I, and theory based on $\chi = 14.8$.

The criterion of 95% transmission used in Method I to determine phase boundaries is somewhat arbitrary. An alternative procedure is to measure the protein concentration in the supernatant using spectrophotometry after centrifuging off the dense complex phase (Method II). For one-phase samples, this concentration should be equal to the total protein concentration, whereas, for two-phase systems, it will be lower, since part of the protein molecules are in the dense complex phase. Thus, we should be able to determine the phase boundary by locating the break in the curve of the supernatant protein concentration versus the total protein concentration.

Figure 2 shows typical results of this procedure at ionic strengths of 10 and 20 mM, and for lysozyme/succinylated lysozyme mixing ratios of 1:9, 1:1, and 9:1. The break in the curves is especially distinct for a mixing ratio of 1:1. This behavior is reminiscent of that of a poorly soluble salt: above a certain solubility limit, all of the additional ions go into the crystal phase. For our case, even at a 1:1 mixing ratio, the positive slope of the curves beyond the phase boundary indicates that not all of the additional protein molecules go into the complex phase. Most likely, this is due to deviations from perfect symmetry: because of the slightly larger molecular weight of succinylated lysozyme, at a mixing ratio of 1:1 (by weight), the numbers of succinylated and nonsuccinylated lysozyme molecules are not exactly equal. Also, the charges of the two kinds of molecules are not exactly equal in magnitude. We will return to this issue in the section titled Comparison of Model and Experiments.

At more asymmetric mixing ratios, the break in the curves is much less pronounced since it is obscured by the high concentration of the species that is in excess. Therefore, the present method is especially useful for a symmetric mixing ratio. Nevertheless, even at mixing ratios 1:9 and 9:1 we still clearly find that above a certain critical concentration, the supernatant concentration is less than the total protein concentration. There is a small but significant difference between the data for 1:9 and those for 9:1 mixing ratios, which is again most likely related to the fact that the number concentrations as well as the charge magnitude are not exactly equal.

(13) van der Veen, M.; Norde, W.; Cohen Stuart, M. A. *Colloids Surf., B* **2004**, *35*, 33.
(14) Biesheuvel, P. M.; van der Veen, M.; Norde, W. *J. Phys. Chem. B* **2005**, *109*, 4172.
(15) Cohen Stuart, M. A.; Besseling, N. A. M.; Fokkink, R. G. *Langmuir* **1998**, *14*, 6846.

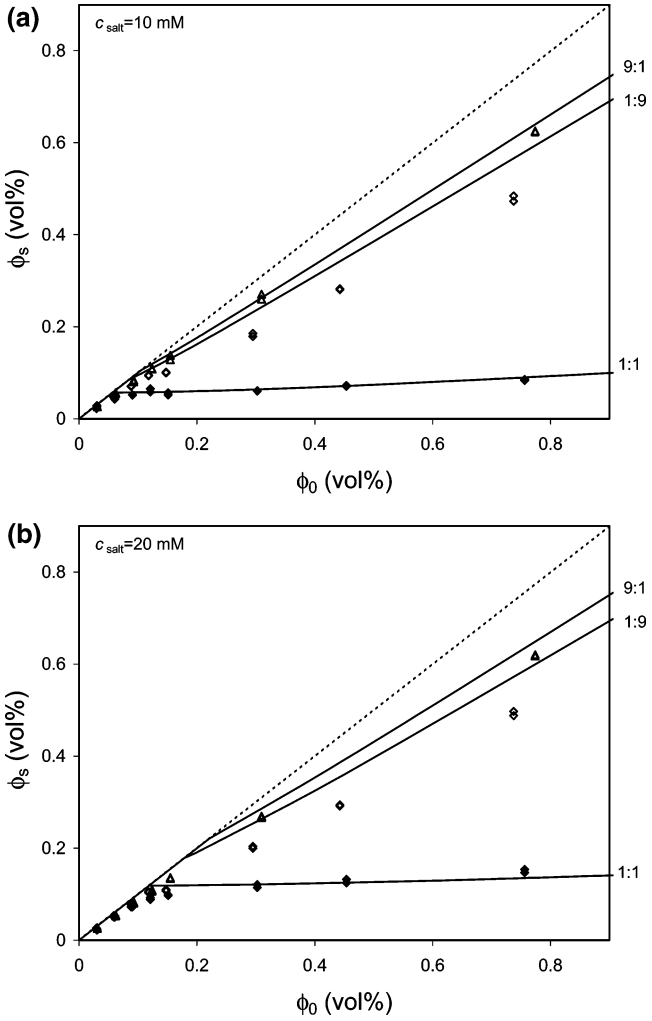

Figure 2. Protein concentration in supernatant, ϕ_s, as a function of total protein concentration, ϕ_0, mixing ratio, and ionic strength. (a) 10 mM. (b) 20 mM. Symbols represent the experimental data (closed diamonds: 1:1 mixing ratio of lysozyme to succinylated lysozyme; open diamonds: 1:9; triangles: 9:1). Deviations from the dotted curve ($\phi_s = \phi_0$) indicate complexation. Solid curves: predictions of the thermodynamical model (discussed in the Theory section; $\chi = 14.0$).

To reduce the number of parameters, we restrict ourselves in the following experiments to symmetric systems (mixing ratio 1:1), for which complexation is most distinct. First we consider the influence of ionic strength. Figure 3 shows the supernatant concentration versus the total protein concentration for a wide range of values of the ionic strength. Again, the data show a transition at a critical protein concentration ϕ_0, indicating the onset of phase separation. With increasing ionic strength, this phase boundary shifts to higher protein concentrations.

A detailed theoretical approach to describe the influence of ionic strength will be discussed in the next section. Here, we first use a more qualitative argument that highlights the origin of the ionic strength dependence, which, to a first approximation, is due to the influence of the small ions on the chemical potential of the protein molecules in solution, whereas the chemical potential of the complexed molecules in the dense phase is not influenced much. Equality of chemical potentials for the two phases in equilibrium implies

$$\mu^+ + \mu^- = \mu^c \tag{1}$$

with "+" and "−" referring to the positively charged and

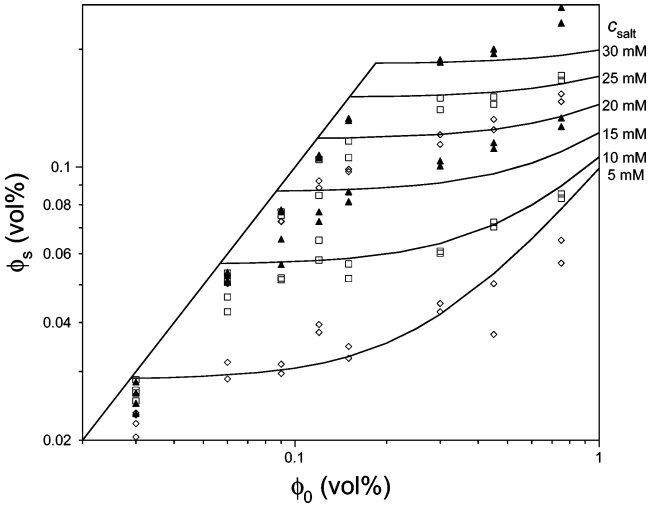

Figure 3. Protein concentration in supernatant as a function of total protein concentration and ionic strength (theoretical curves based on $\chi = 14.0$; experiments based on Method II; 1:1 mixing ratio).

negatively charged protein molecules in solution, and "c" referring to the complex phase that is assumed to contain equal numbers of both molecules. Inspired by the analogy with poorly soluble salts, we here make the approximation that μ^c is independent of ionic strength for the protein complexes. To calculate the ionic strength dependence of the chemical potential of the protein molecules in solution, we assume that the molecules are far apart (relative to the Debye length). For low surface potentials, the chemical potential is then given by

$$\mu^i = \ln c_i + \frac{Z^2}{2}\frac{\lambda_B}{a(1+\kappa a)} \tag{2}$$

The second, electric, term is equal to $^1/_2 \cdot Z \cdot y$, where y is the dimensionless surface potential (also see Theory section), c_i is the protein concentration, Z is the charge of the molecule, λ_B is the Bjerrum length (= 0.72 nm in water), κ^{-1} is the Debye length, $\kappa^2 = 8\pi\lambda_B n_\infty$ (we assume throughout that all small ions are monovalent), and n_∞ is the ionic strength (in m^{-3}; $= c_\infty \cdot N_{av}$, with c_∞ in mM). Combining eqs 1 and 2, and assuming that Z is equal in magnitude for both molecules, we obtain an expression for the equilibrium constant

$$K = c^+ c^- = \exp\left\{\mu^c + Z^2 \frac{\lambda_B}{a(1+\kappa a)}\right\} \tag{3}$$

The simplified model can be checked using experimentally determined phase boundaries, at which the protein concentrations in solution, c^+ and c^-, are known. We use the data of Figure 1 (at a fixed total protein concentration but varying mixing ratio), while, for the data of Figure 3 (at a fixed mixing ratio of 1:1, but for varying total protein concentration), we estimated the phase boundary from extrapolating from data clearly in the 2ϕ region back to the 1:1 line (which corresponds to absence of phase separation). Results of the analysis are shown in Figure 4. The data indeed suggest the correct dependence on κ and thus on ionic strength. Differences between the two data sets are not entirely unexpected because the two experimental methods are so different. From the slope of the curves, we can estimate a corresponding protein charge Z, which results in $Z \sim 5-6$, which is somewhat lower than the expected value of $Z \sim 7$ (taken from acid/base titration) but is not unreasonable, given the approximate nature of this analysis, in which the influence of the ionic strength on the chemical potential μ^c of the protein molecules in the

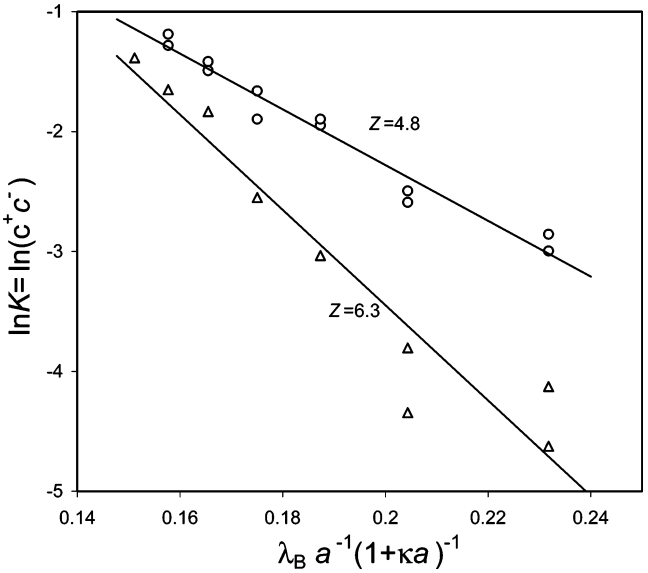

Figure 4. Ionic strength dependence of the solubility product $K = c^+c^-$ of protein complexes. The triangles are based on the data of Figure 1, and the circles are based on the data in Figure 3. The solid lines are based on eq 3 with Z the fitted values of the protein charge.

complex phase is neglected. This additional element will be incorporated in the Theory section.

Finally, we investigated the temperature dependence of the phase boundaries (Method III). Results are presented in Figure 5, which shows the temperature at which the opaque solutions became completely transparent, T_{clarify}. Because the electrostatic interactions between the protein molecules are not expected to be particularly sensitive to temperature, the observed sensitivity to temperature suggests an additional nonelectrostatic attraction that is quite sensitive to temperature.

Theory

Modeling the phase behavior of mixtures of oppositely charged macromolecules has a long history (reviewed in ref 16), starting with the work on the complex coacervation of oppositely charged flexible polyelectrolytes by Overbeek and Voorn.[17] An important theoretical problem is that the electrostatic contribution to the free energy sensitively depends on the spatial correlations of the positively and negatively charged macromolecules. Depending on the strength of the electrostatic interactions, spatial correlations may vary from very weak to extremely strong. Estimating the nonelectrostatic contribution to the free energy (assuming that these contributions can be separated) is less problematic and can be done using a variety of well-known approximations.

Weak-coupling approximations, for systems with weak spatial correlations, have been around for a long time: the Overbeek−Voorn approximation falls into this category, as well as random-phase approximations for weakly charged polyelectrolytes of opposite charge.[18,19]For stronger correlations, a possibility is to estimate the electrostatic contribution to the free energy on the basis of a plausible assumption for the spatial organization of the complex. Along these lines, we recently developed a heterogeneous PB cell model (see Figure 6) to estimate the electrostatic free energy of strong complexes of oppositely charged flexible polyelectrolytes.[4] In the present work, we will extend

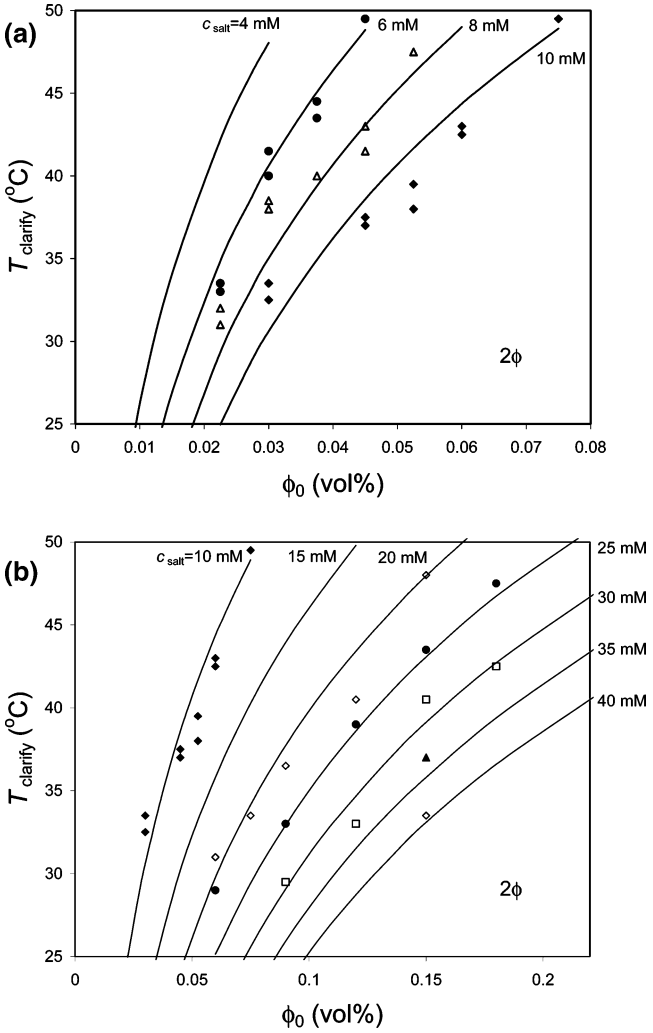

Figure 5. T_{clarify} as a function of total protein concentration for various ionic strengths. (a) circles: 6 mM; triangles: 8 mM; diamonds: 10 mM. (b) closed diamonds: 10 mM; open diamonds: 20 mM; circles: 25 mM; squares: 30 mM; triangle: 35 mM; diamond 40 mM. Full curves are based on the thermodynamical theory (discussed in the Theory section; χ from eq 29).

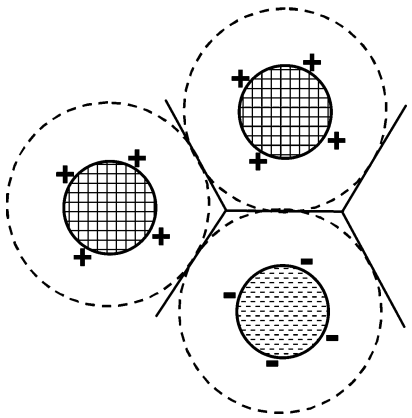

Figure 6. Schematic of heterogeneous cell model for a mixture of positively and negatively charged spherical colloids. In the envelopes between the charged surface of the colloid (solid line) and the (virtual) edge of the cell (dashed line), the PB equation is solved in spherical coordinates. At the edge of the cell, each colloid interacts with the mean-field environment.

that approach to mixtures of oppositely charged spheres to describe the electrostatic interaction between mixtures of globular protein molecules.

(16) de Kruif, C. G.; Weinbreck, F.; de Vries, R. *Curr. Opin. Colloid Interface Sci.* **2004**, *9*, 340.
(17) Overbeek, J. Th. G.; Voorn, M. J. *J. Cell. Comp. Physiol.* **1957**, *49*, 7.
(18) Kudlay, A.; Olvera de la Cruz, M. *J. Chem. Phys.* **2004**, *120*, 404.
(19) Kudlay, A.; Ermoshkin, A. V.; Olvera de la Cruz, M. *Macromolecules* **2004**, *37*, 9231.

Generally, in cell models, envelopes of solvent plus small ions are envisioned around each charged colloid or molecule. Each cell consists of one charged sphere plus the solvent envelope. The PB equation is solved for the space between colloid and cell edge. In one-component PB cell models, the boundary condition at the edge of a cell is fixed by the requirement that each cell in itself is electroneutral.[20−23] Such homogeneous cell models are well-established for one-component systems in which the colloids or molecules are repulsive and can be expected (when concentrated enough) to distribute in such a way as to maximize the interparticle distance, that is, to form a packing with a well-defined interparticle distance.

Heterogeneous cell models, to be used for mixed systems (thus, with different kinds of particles), are much less well-established but have found use in describing drag forces in mixtures of (uncharged) particles of different size moving under an external force.[24,25] For oppositely charged particles, the applicability of heterogeneous cell models may seem problematic, since interparticle distances between particles of opposite charge may be very different from those between particles of equal charge. However, in a strong complex, the density may be so high that the interparticle distances again become fairly uniform. The heterogeneous cell model also applies to very dilute mixtures of noninteracting charged spheres because it correctly gives the electrostatic free energy of the electric double layer surrounding isolated charged spheres. Deviations are expected to be largest at intermediate sphere densities. However, phase separation often occurs between dilute and very concentrated phases, and, for both of these, the heterogeneous cell model is expected to be reasonable.

Therefore, we consider a mixture of colloidal spheres of fixed charge, Z^+ and Z^- (not necessarily of equal magnitude), and equal volume, v, in an aqueous solution containing small ions. For the small ions, we assume a fixed chemical potential (grand canonical) as if the system is in equilibrium with a large aqueous solution via a membrane permeable to the small ions (and solvent), but not to the charged spheres.

Nonelectrostatic Contribution. As mentioned, we assume that the total free-energy density f separates into an electrostatic and a nonelectrostatic contribution

$$f = f_{\mathrm{el}} + f_{\mathrm{non-el}} \tag{4}$$

The nonelectrostatic contribution is approximated using a Carnahan−Starling−van der Waals equation-of-state (EOS). This is a modification of the classical van der Waals EOS obtained by replacing the van der Waals repulsive term by the Carnahan−Starling expression.[26] In this part of the model, where electrostatic interactions are not considered, the oppositely charged spheres are assumed to be identical. Then the free-energy density takes the form

$$f_{\mathrm{non-el}}v = \sum_i \phi_i \ln \phi_i + \frac{4\phi^2 - 3\phi^3}{(1-\phi)^2} - \chi\phi^2 \tag{5}$$

while the contribution to the osmotic pressure is

$$\Pi_{\mathrm{non-el}}v = \phi\frac{1 + \phi + \phi^2 - \phi^3}{(1-\phi)^3} - \chi\phi^2 \tag{6}$$

and the contribution to the chemical potential is given by

$$\mu_{i,\mathrm{non-el}} = \ln \phi_i + \frac{\phi(8 - 9\phi + 3\phi^2)}{(1-\phi)^3} - 2\chi\phi \tag{7}$$

Similar thermodynamic functions have been used previously for (one-component) protein solutions (e.g., in refs 27 and 28). In the above equations, ϕ is the overall volume fraction of protein molecules, and ϕ_i is the volume fraction of each individual component, while all thermodynamic functions are scaled to the thermal energy, kT. Note that, in eqs 5 and 7, the individual volume fractions only enter in the ideal entropy term, $\ln \phi_i$. As mentioned, our experiments indicate the presence of an additional, nonelectrostatic attraction that is temperature dependent. This is included in the model (at the van der Waals level) via the parameter χ.

Electrostatic Contribution. To estimate the electrostatic contribution to the free-energy density, we set up a heterogeneous PB cell model. For a binary mixture, two different kinds of spherical cells are considered (see Figure 6). The electrostatic potential is continuous; hence, all cells have a common value of the electrostatic potential at the cell boundary. The fields strengths at the boundaries of the two kinds of cells need not be the same. Therefore the individual cells are not necessarily electroneutral. Instead, the field strengths at the cell boundaries are self-consistently obtained from the requirement of overall electroneutrality of all cells together. This amounts to averaging the field strength over the surfaces of the cells. In other words, the cells "see" a mean-field surrounding, with a excess charge that exactly cancels their own net charge.

For N_1 spheres of type one and N_2 spheres of type two, overall electroneutrality results in

$$N_1 b_1^2 \frac{\mathrm{d}y}{\mathrm{d}r}\Big|_{b_1,\mathrm{cell1}} + N_2 b_2^2 \frac{\mathrm{d}y}{\mathrm{d}r}\Big|_{b_2,\mathrm{cell2}} = 0 \tag{8}$$

with b_i being the outer cell radius, r being the radial coordinate in each cell, and y being the dimensionless electrostatic potential, which is related to the electrostatic potential ψ according to $y = e\psi/kT$, where e is the electronic charge.

In principle, we have complete freedom in dividing the available volume over the two kinds of cells. However, especially for symmetric systems, the most appropriate approximation seems to be to assume that the outer cell radii of the two kinds of cells are equal. Then the volume of each cell is simply the inverse of the total particle number density, ρ. The radius of the spherical molecule, a, and the outer radius of the cell, $b = b_i$, are thus related to the volume density of all spheres combined, ϕ, according to

$$\phi = \frac{a^3}{b^3} \tag{9}$$

Combining eqs 8 and 9 results in

$$\phi_1 \frac{\mathrm{d}y}{\mathrm{d}r}\Big|_{b,\mathrm{cell1}} + \phi_2 \frac{\mathrm{d}y}{\mathrm{d}r}\Big|_{b,\mathrm{cell2}} = 0 \tag{10}$$

where ϕ_i is the volume fraction of component i.

(20) Alexander, S.; Chaikin, P. M.; Grant, P.; Morales, G. J.; Pincus, P.; Hone, D. *J. Chem. Phys.* **1984**, *80*, 5776.
(21) Hansson, P. *Langmuir* **2001**, *17*, 4167.
(22) Allen, R. J.; Warren, P. B. *Langmuir* **2004**, *20*, 1997.
(23) Biesheuvel, P. M.; Wittemann, A. *J. Phys. Chem. B* **2005**, *109*, 4209.
(24) Patwardhan, V. S.; Tien, C. *Chem. Eng. Sci.* **1985**, *40*, 1051.
(25) Biesheuvel, P. M.; Verweij, H.; Breedveld, V. *AIChE J.* **2001**, *47*, 1969.
(26) Carnahan, N. F.; Starling, K. E. *AIChE J.* **1972**, *18*, 1184.
(27) Berland, C. R.; Thurston, G. M.; Kondo, M.; Broide, M. L.; Pande, J.; Ogun, O.; Benedek, G. B. *Proc. Natl. Acad. Sci.* **1992**, *89*, 1214.
(28) Taratuta, V. G.; Holschbach, A.; Thurston, G. M.; Blankschtein, D.; Benedek, G. B. *J. Phys. Chem.* **1990**, *94*, 2140.

Phase equilibrium computations are more complicated when the thermodynamic functions must be determined numerically. Therefore, instead of using the full nonlinear PB equation, here we analytically compute the electrostatic free-energy density of our cells using the Debye−Hückel approximation of linearizing the PB equation. For typical solutions of globular proteins, at moderate ionic strengths, this is not unreasonable. Also, it should be noted that the heterogeneous cell model itself is already quite a drastic approximation, such that it is not certain that using the full PB equation would make the theory much more accurate.

The derivation of the thermodynamic functions Π and μ is analogous to that in ref 23 (eqs 11−20) in which a one-component system is considered (homogeneous cell model) on the basis of the PB equation in the low-potential limit in spherical coordinates

$$\frac{1}{r^2}\frac{\mathrm{d}}{\mathrm{d}r}r^2\frac{\mathrm{d}y}{\mathrm{d}r} = \kappa^2 y \tag{11}$$

to be solved in the annular space $a < r < b$. The boundary condition at b is given by eq 10, while at the surface of the colloidal sphere ($r = a$)

$$\frac{\mathrm{d}y}{\mathrm{d}r} = -\frac{Z\lambda_\mathrm{B}}{a^2} \tag{12}$$

Equation 11 has the general solution[29]

$$y = \frac{ay_\mathrm{a}}{r}\cosh(\kappa r - \kappa a) + \frac{by_\mathrm{b} - ay_\mathrm{a}\cosh(\kappa b - \kappa a)}{r\sinh(\kappa b - \kappa a)}\sinh(\kappa r - \kappa a) \tag{13}$$

Solving the heterogeneous cell model, we find for the electrostatic potential, y_i, at the colloid surface, $r = a$, in cell i

$$y_i = \frac{\kappa\lambda_\mathrm{B}}{\mathrm{th} + \kappa a}\left(\frac{\mathrm{th}}{\kappa a}Z_i + (1 - \mathrm{th}^2)\frac{Q_1}{\phi}\sum_i Z_i\phi_i\right) \tag{14}$$

where

$$Q_1 = \left(1 - \frac{a}{b} - \left(\frac{1}{\kappa b} - \kappa a\right)\mathrm{th}\right)^{-1} \tag{15}$$

and

$$\mathrm{th} = \tanh(\kappa b - \kappa a) \tag{16}$$

In the Debye−Hückel low-potential limit, the electrostatic contribution to the free-energy density f is given by (all molecules/colloids have volume υ)

$$f_\mathrm{el}\upsilon = \frac{1}{2}\sum_i \phi_i Z_i y_i \tag{17}$$

which, with eq 14, results in

$$f_\mathrm{el}\upsilon = \frac{\kappa\lambda_\mathrm{B}}{2(\mathrm{th} + \kappa a)}\left(\frac{\mathrm{th}}{\kappa a}\sum_i \phi_i Z_i^2 + \frac{Q_1}{\phi}(1 - \mathrm{th}^2)\left(\sum_i Z_i\phi_i\right)^2\right) \tag{18}$$

The colloid osmotic pressure Π is related to the free-energy density according to

$$\Pi_\mathrm{el} = \phi^2\frac{\mathrm{d}}{\mathrm{d}\phi}\frac{f_\mathrm{el}}{\phi} \tag{19}$$

which, for Π, results in

$$\Pi_\mathrm{el}\upsilon = \frac{\kappa^2 b\lambda_\mathrm{B}}{6}\frac{1 - \mathrm{th}^2}{(\mathrm{th} + \kappa a)^2}\cdot\left[\frac{Q_1Q_2}{\phi}\left(\sum_i \phi_i Z_i\right)^2 - \sum_i \phi_i Z_i^2\right] \tag{20}$$

with

$$Q_2 = 2\mathrm{th}(\mathrm{th} + \kappa a) + 1 - \mathrm{th}^2 + Q_1(\mathrm{th} + \kappa a)\left(\frac{a}{\kappa b^2} + \frac{1}{\kappa^2 b^2}\mathrm{th} - \left(\frac{1}{\kappa \mathrm{b}} - \kappa a\right)(1 - \mathrm{th}^2)\right) \tag{21}$$

The electrostatic contribution to the chemical potential of species i, is given by

$$\mu_{i,\mathrm{el}} = \upsilon\left.\frac{\mathrm{d}f_\mathrm{el}}{\mathrm{d}\phi_i}\right|_{\phi_j} \tag{22}$$

where the subscript ϕ_j refers to the differentiation being performed for constant volume fractions of all other colloidal species. Equation 22 results in

$$\mu_{i,\mathrm{el}} = \frac{1}{2}\frac{Z_i^2\lambda_\mathrm{B}}{a}\frac{\mathrm{th}}{\mathrm{th} + \kappa a} + \frac{Q_1\kappa\lambda_\mathrm{B}}{2\phi}\left(Z_i - (Z_j - Z_i)\frac{\phi_j}{\phi}\right)\frac{1 - \mathrm{th}^2}{\mathrm{th} + \kappa a}\sum_i \phi_i Z_i + \Pi\frac{\upsilon}{\phi} \tag{23}$$

or

$$\mu_{i,\mathrm{el}} = \frac{1}{2}Z_i y_i - \frac{Q_1\kappa\lambda_\mathrm{B}}{2\phi^2}(Z_j - Z_i)\phi_j\frac{1 - \mathrm{th}^2}{\mathrm{th} + \kappa a}\sum_i \phi_i Z_i + \frac{\kappa^2 b\lambda_\mathrm{B}}{6\phi}\frac{1 - \mathrm{th}^2}{(\mathrm{th} + \kappa a)^2}\cdot\left[\frac{Q_1Q_2}{\phi}\left(\sum_i \phi_i Z_i\right)^2 - \sum_i \phi_i Z_i^2\right] \tag{24}$$

Equation 24 gives the electrostatic contribution to the chemical potential of component i in a certain phase as a function of the electrostatic potential y_i from eq 14, the volume fractions ϕ_1 and ϕ_2, and the geometrical factors Q_1 and Q_2 from eqs 15 and 21. These factors depend only on the cell radii a and b (thus on the total volume fraction, ϕ), and the Debye length, κ^{-1}.

Phase Behavior. To determine the phase diagram, we solve the usual set of equations: equality of the chemical potential of each species in the two phases (with the contribution of eqs 7 and 24) and equality of the colloid osmotic pressure (with contributions from eqs 6 and 20). We need to solve these equalities together with expressions for the surface potentials, eq 14, and the conservation of mass,

$$\phi_{i,0} = \phi_{i,\mathrm{c}}\zeta + \phi_{i,\mathrm{s}}(1 - \zeta) \tag{25}$$

where ζ is the relative volume of the complex (c) phase, s refers to the solution phase, and 0 refers to the overall amount of component i (per unit volume).

To illustrate the theory, here we consider a limiting case for which the expressions simplify considerably: a stoichiometric mixture (i.e., $\phi_{i,0} = {}^1/_2\cdot\phi_0$) of spherical particles having exactly opposite charges, $\pm Z$. In this case, and with a symmetric form of the nonelectrostatic forces, stoichiometry is preserved in the coexisting phases (i.e., in both phases, we always have equal amounts of the two types of particles), such that we have a quasi

(29) Zydney, A. L. *J. Colloid Interface Sci.* **1995**, *169*, 476.

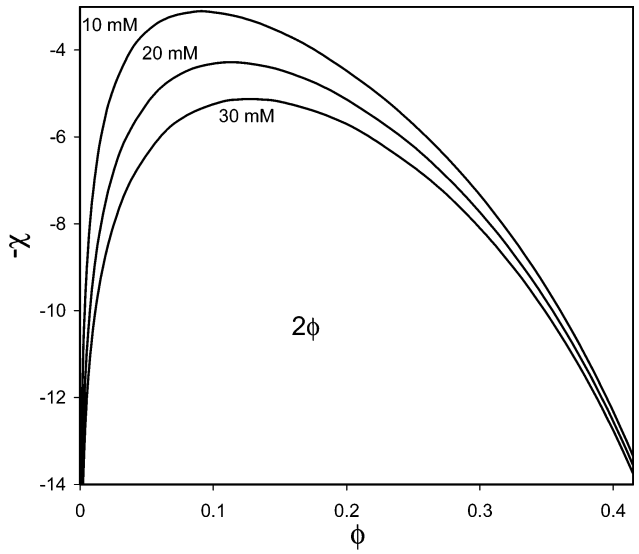

Figure 7. Phase diagram for a quasi one-component, symmetric system ($Z^+ = -Z^- = 7$; $\phi_i = {}^1/_2{\cdot}\phi$, $\upsilon = 37$ nm^3) as function of χ (describing the attraction between the colloids) and ionic strength.

one-component system. The electrostatic potential at the sphere surface becomes

$$|y_i| = \frac{\lambda_B \cdot \mathrm{th} \cdot Z}{a(\mathrm{th} + \kappa a)} \tag{26}$$

whereas, for the electrostatic contribution to the colloid osmotic pressure, we now find

$$\Pi_{el}\upsilon = -\kappa^2 b \lambda_B \frac{\phi Z^2}{6} \frac{1 - \mathrm{th}^2}{(\mathrm{th} + \kappa a)^2} \tag{27}$$

while the electrostatic contribution to the chemical potential μ (equal for both components) simplifies to

$$\mu_{el} = \frac{\kappa \lambda_B Z^2}{\mathrm{th} + \kappa a}\left(\frac{\mathrm{th}}{2\kappa a} - \frac{1 - \mathrm{th}^2}{\mathrm{th} + \kappa a}\frac{\kappa b}{6}\right) \tag{28}$$

For this quasi one-component system we can now easily construct a $\phi-\chi$ phase diagram after combining eqs 27 and 28 with eqs 6 and 7 ($\phi_i = \phi/2$), resulting in two equations and the two unknown coexisting volume densities, ϕ. The strength of the attraction, that is, $-\chi$, essentially plays the role of "temperature" (on the y-axis). Figure 7 shows the basic features of phase separation as predicted by our theory: at high attraction (low $-\chi$), phase separation can be observed; the region of phase separation expands with decreasing ionic strength, which is due to the increased electrostatic attraction between oppositely charged spheres at lower ionic strength.

The density of the complex phase (high-density branch) shows values in the 30−40 vol % range, in line with the dense phase volume fractions measured by Liu et al.[11,12] for aqueous mixtures of two types of γ-crystallin. Figure 7 resembles a phase diagram for polymers under poor solvent conditions. Note that, except for the region close to the critical point, the equilibrium is indeed between a concentrated and a dilute phase, and we expect the heterogeneous PB cell model to be reasonable for both.

Comparison of Model and Experiments

Next we apply the theory to our experimental data of the phase separation of lysozyme and succinylated lysozyme. Both protein molecules are approximated as spherical colloids of volume $\upsilon = 37$ nm^3 (see ref 30 for lysozyme), which corresponds to a radius of $a = 2.07$ nm. The fixed charge on the protein molecules is assumed to be a function of both pH and ionic strength, but not of protein concentration. These charges are computed from the classical Tanford titration model[31] for lysozyme and succinylated lysozyme that we described in detail in ref 14. The molecule is assumed to be spherical, and the solution is assumed to be sufficiently dilute that the diffuse layers around different molecules do not overlap. The titration model quite accurately fits experimental titration curves for the two protein molecules.[14] Predicted isoelectric points are pI = 10.7 for lysozyme and pI = 4.7 for succinylated lysozyme, in agreement with experiment.

Neglecting the influence of protein concentration on the charges of the proteins is presumably a good approximation, since, at the experimental pH of 7.5, both proteins have a local plateau in their titration curves[13,14] such that they very nearly behave as if they had a fixed charge, Z. Clearly, close to the isoelectric points of the proteins, the fixed charge approximation is no longer accurate. At pH 7.5, the predicted charges are, at infinite ionic strength, $Z^+ = +8.07$ and $Z^- = -6.89$ for lysozyme and succinylated lysozyme, respectively. At the ionic strengths used in the experiments, the charge is somewhat lower, ranging from $Z^+ = 7.85$ and $Z^- = -6.62$ at 6 mM to $Z^+ = 7.94$ and $Z^- = -6.75$ at 40 mM. All parameters are fixed, except for the nonelectrostatic attraction, χ, which we use as the only adjustable parameter in our comparison with the experimental data.

In Figure 1, the theory is tested against the protein titration data, and, using a value of $\chi = 14.8$, we find excellent agreement with the data. Note that both the experiment and the theory show that, in the present system, phase separation is possible, even at extremely asymmetric mixing ratios. As discussed earlier, this is most likely due to the fact that the experimental system is nearly symmetric, both in charge and geometry.

Next, consider the experiments in which we spectrophotometrically determine the protein concentration in the supernatant, ϕ_s, after centrifugation (Method II; see Figures 2 and 3). In comparing with the theory, we identify ϕ_s with the volume fraction of protein molecules in the solution phase in the case of a two-phase coexistence. Here, we find that a value of $\chi = 14.0$ gives a very good fit of the model to the data. First, consider the effect of the mixing ratio, as shown in Figure 2 (for ionic strengths of 10 and 20 mM). The theory exactly reproduces the fact that the 9:1 situation results in a higher ϕ_s (lower amount complexed) than does the 1:9 situation because of the slight asymmetry of the charges on the lysozyme and succinylated lysozyme (lysozyme has a higher charge) and the fact that molar mixing ratios are different from mass ratios (resulting in a higher number for the lighter lysozyme molecule). Because of these two effects, the 1:9 case is closer to a 1:1 symmetry than is the 9:1 case. The theory also exactly reproduces the finding that the ionic strength has a significant influence on the amount complexed at a 1:1 mixing ratio, but has no influence at 1:9 and 9:1 ratios. The situation at a 1:1 mixing ratio is not unexpected: with increasing ionic strength, the chemical potential of the molecules in solution is lowered, and therefore complexation diminished. However, for the asymmetric mixing ratios, we have no ready explanation for the invariance of the complexed amount to ionic strength (as observed both in the experiment and in theory).

Having identified that complexation is most pronounced at symmetric mixing ratios (which in itself is not very surprising),

(30) González Flecha, F. L.; Levi, V. *Biochem. Mol. Biol. Edu.* **2003**, *31*, 319.
(31) Tanford, C.; Swanson, S. A.; Shore, W. S. *J. Am. Chem. Soc.* **1955**, *77*, 6414.

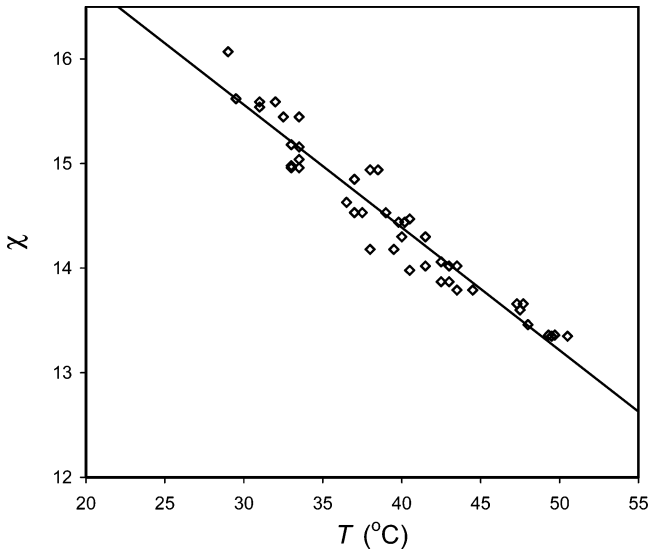

Figure 8. Temperature dependence of interaction parameter χ.

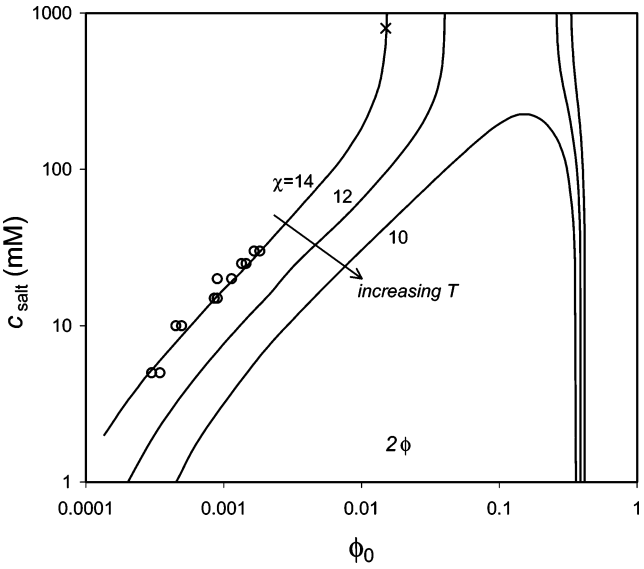

Figure 9. Ionic strength vs total protein concentration phase diagram as a function of temperature.

we continue with experiments at a 1:1 mixing ratio (this is a mass mixing ratio; in number densities, this translates to 51.53% of all molecules being lysozyme). The results are shown in Figure 3. The straight 1:1 line represents the situation in which all protein is in solution, as expected in the absence of phase separation. The minimum protein concentration required for phase separation to occur increases with increasing ionic strength (phase separation is "more difficult" at high ionic strength). Though the onset of phase separation in the experiment is not as sharp as the theory predicts, we again find a remarkable agreement, with the dependencies on ϕ_0 and ionic strength being very well reproduced. The theory also predicts that, upon increasing ϕ_0 beyond the phase separation threshold, the protein concentration in the supernatant ϕ_s first remains constant (plateau region), but then starts increasing at higher ϕ_0, especially at low ionic strength. The experimental data also show an increase in ϕ_s after a plateau region, especially at low ionic strength. However, the dependence of this effect on ionic strength is not as pronounced as predicted by the theory. The increase of ϕ_s after the plateau region is due to the slight imbalance in charges between Z^+ and Z^-, excluding a small and constant fraction of all protein from the dense phase. If the molecules would be of exactly opposite charge and present in equal numbers, the plateau region would extend all the way up to values of ϕ_0 in the 30−40 vol % range where we enter the one-phase region again.

Finally, we consider the experiments in which we determine T_{clarify}, the temperature beyond which the solution becomes clear to the eye. As mentioned, the temperature dependence of the phase behavior is presumably caused by a temperature-dependent, nonelectrostatic attraction. In other words, we expect χ to be a function of temperature, and, from the measurements of T_{clarify}, we ideally would like to determine this correlation. This has been done in the following way: First note that the experimental T_{clarify} corresponds to the situation in which the attraction χ is just strong enough for phase separation. In each experiment (defined by ionic strength, protein mixing ratio, and concentration), we calculate the theoretical value of χ corresponding to the onset of phase separation. Thus, we obtain a set of $T_{\text{clarify}}-\chi$ coordinates (see Figure 8). If our thermodynamical model is accurate, and if the temperature-dependent attraction parameter is indeed independent of ionic strength, protein concentration, and mixing ratio, all $T-\chi$ points should fall on a common master curve. This indeed turns out to be quite nearly the case, as is shown in Figure 8. Using the $\chi(T)$ correlation

$$\chi = 19 - 0.115T \tag{29}$$

with T in °C (shown as a solid line in Figure 8), we can predict T_{clarify} for arbitrary values of the total protein concentration and ionic strength and, as expected, find excellent agreement between theory and experiment, as is shown in Figure 5. For instance, the increasing slope of the curves with decreasing ionic strength is very well reproduced.

To construct a phase diagram as a function of total protein concentration and ionic strength at a 1:1 mixing ratio, we use the phase boundaries determined by estimating the positions of the breaks in the curves of Figure 3 (by extrapolating from the data at concentrations clearly in the phase-separation regime back to the intersection with the 1:1 line that represents the absence of phase separation). These points (circles) are plotted in Figure 9. Also, in quasi-elastic light scattering experiments, we find that, at a total protein concentration of 10 g/L, the critical ionic strength for phase separation is around 800 mM.[32] This single data point is indicated as a cross in Figure 9. As is evident, the calculated phase diagram is in excellent agreement with the experimental results.

At high ionic strength, electrostatics no longer influences the phase behavior, which results in the vertical slopes of the phase boundary in Figure 9 (for $\chi = 14$). In this nonelectrostatic regime, we have only a competition between entropy, excluded volume, and the nonelectrostatic attraction. For the fitted value of the nonelectrostatic attraction, $\chi = 14$, theory predicts that the dense phase always has a very high density, on the order of ∼35 vol % (in line with the experimental data for mixtures of two types of γ-crystallin[11,12]). When we increase the temperature in the model we find at sufficiently high temperatures (corresponding to sufficiently low values of the attraction χ) a closed phase boundary. In this case, we can always go to the one-phase region by adding salt (irrespective of ϕ_0) and obtain a one-phase system with protein concentrations between, for instance, 5 and 25 vol %, which is impossible at $\chi = 14$ (room temperature).

For completeness, we also show phase diagrams as a function of ionic strength and colloid charge (see Figure 10). In the phase

(32) Lindhoud, S., M.S. Thesis, Wageningen University, 2005.

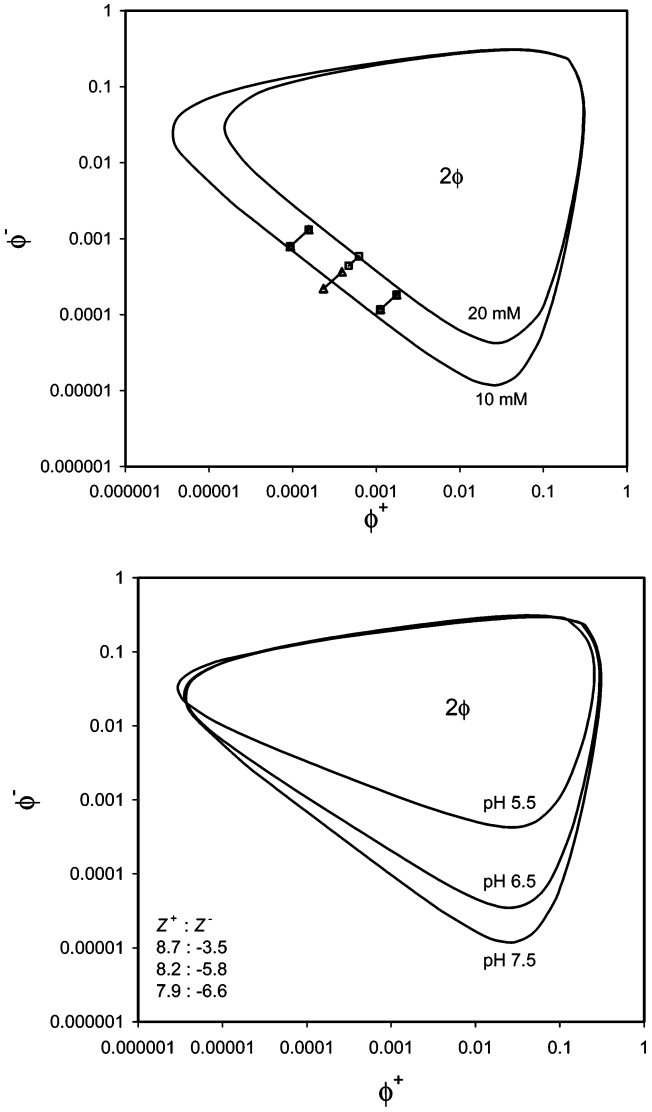

Figure 10. Phase diagram as a function of (a) ionic strength (pH 7.5) and (b) colloid charge (thus as a function of pH; $c_\infty = 10$ mM). Phase separation occurs within the region enclosed by the coexistence curves. Data points correspond to the onset of phase separation in Figure 2.

diagram as a function of ionic strength, Figure 10a, we have also included experimental phase boundaries estimated from the data of Figure 2. Unfortunately, for the asymmetric mixing ratios (9:1 and 1:9), the estimates are not very reliable (triangles represent the 10 mM case; squares represent 20 mM). Figure 10b illustrates the influence of pH on the phase separation. With decreasing pH, the charge on the lysozyme slightly increases, but the charge on the succinylated lysozyme becomes much less negative. As a consequence, the two-phase (2ϕ) region shrinks in an asymmetric fashion, and, for phase separation, higher protein concentrations are required.

Discussion

We would like to discuss a number of issues relating to the fitted values of the interaction parameter χ. First, fitting the theory to the data gave different χ values for the different kinds of experiments: $\chi = 14.8$ from turbidity (Method I), $\chi = 14.0$ from protein supernatant concentration (Method II), and $\chi \sim 16$ from T_{clarify} by Method III (when extrapolated to 25 °C). The latter value is the highest, possibly because a rather stringent criterion was used to assess clarification, namely that the sample became completely clear to the eye, whereas the criterion of 95% transmission in Method I corresponds already to a slightly turbid sample. Taking a less stringent criterion in Method III would shift the data in Figure 8 to the left, thereby lowering χ. The criterion of 95% percent transmission (used in Method I) is also somewhat arbitrary and may affect the reliability of the value of $\chi = 14.8$ determined from the data in Figure 1. In short, we think that the most accurate estimate of the attraction comes from fitting the Method II data for the concentration of protein in the supernatant after centrifugation, $\chi = 14.0$. Nevertheless, all values are of the same order of magnitude, and the two most reliable ones are within a 10% margin.

Prinsen and Odijk[33] argue that interactions between globular proteins, particularly between lysozyme molecules, are fairly well represented by a sum of steric repulsion, electrostatic interactions, plus a short-ranged, nonelectrostatic attraction, presumably due to hydrophobic interactions and hydrogen bonding. Since we assume that succinylation only affects the protein charge, but not the short-ranged, nonelectrostatic attraction between the protein molecules, we should be able to compare our values for the interaction parameter χ with data for lysozyme−lysozyme interactions at high ionic strength (when electrostatic interactions are completely screened). Prinsen and Odijk[33] summarize experimental values of the second virial coefficient, B_2, of lysozyme (dimension nm^3, obtained from $B_2/B_{2,\text{HS}}$ in Figure 2 of ref 33 by multiplying with $B_{2,\text{HS}} = 4\cdot\upsilon$, with υ being the assumed volume of the molecule). At high ionic strength, in Figure 2 of ref 33, reported values for $B_2/B_{2,\text{HS}}$ are between −2.7 and −3.7. This translates into values for B_2 (a protein volume of ∼21 nm^3 is used in ref 33) of 227−311 nm^3. Because the Taylor expansion of eq 6 results in

$$B_2 = \upsilon(4 - \chi) \tag{30}$$

we obtain, with the value for υ used in the present work, namely, $\upsilon = 37$ nm^3, values for χ in the range of ∼15 to ∼19, which are rather close to the values we find for lysozyme−succinylated lysozyme mixtures.

We can also compare the measured temperature dependence of χ, namely $d\chi/dT \sim -0.115$/°C, with that reported in the literature for lysozyme−lysozyme interactions. According to Rosenbaum and Zukoski,[34] B_2 increases with ∼4.2 nm^3/°C (their Figure 5), and according to Petsev et al.,[35] it increases with ∼3.4 nm^3/°C (their Figure 3), which, according to eq 30 and using $\upsilon = 37$ nm^3, results in $d\chi/dT$ in the range of −0.09 to −0.11/°C, again close to the value we derived from our experiments and model.

In future studies we hope to investigate, in more detail, the nature of both the dilute and the dense phases. However, the dense phases are opaque and seem to be very concentrated, as is also suggested by our theoretical model. This makes them different from the "complex coacervate" phases often found in mixtures of globular proteins and oppositely charged polyelectrolytes: these are less dense, transparent, viscous fluids. The difference is most likely caused by the rather strong nonelectrostatic attraction that is generally present between globular proteins. As suggested by our theoretical model, only at much lower values of the nonelectrostatic attraction does one find a closed loop in the phase diagram of Figure 9 and the possibility of less concentrated dense phases.

(33) Prinsen, P.; Odijk, T. *J. Chem. Phys.* **2004**, *121*, 6525.
(34) Rosenbaum, D. F.; Zukoski, C. F. *J. Cryst. Growth* **1996**, *169*, 752.
(35) Petsev, D. N.; Wu, X.; Galkin, O.; Vekilov, P. G. *J. Phys. Chem. B* **2003**, *107*, 3921.

Acknowledgment. We thank Rik Wensink, Kees de Kruif (University of Utrecht), Peter Prinsen (Technical University Delft), and Klaas Besseling (Wageningen University) for useful discussions, and Marijn van der Veen (Wageningen) for introducing us to the succinylation technique. This research was financially supported by NWO, Netherlands Organisation for Scientific Research.

LA052334D